Theoretical Aspects of Photochemical Substitution of $[Mn(CO)_5Cl]$ and Related Complexes†

Kristin Pierloot, Patrick Hoet and Luc G. Vanquickenborne*
Department of Chemistry, University of Leuven, Celestijnenlaan 200F, B-3001 Heverlee-Leuven, Belgium

A self-consistent field analysis of the photolysis of $[Mn(CO)_5Cl]$ has been performed. Based on electron-density difference plots and population analysis a correlation is made between the nature of the photoactive state and the preferential leaving ligand. The stereochemistry of the photolysis reaction has been determined by a study of the possible excited-state isomerization pathways of the five-co-ordinated structure $[Mn(CO)_4Cl]$. The analysis confirms the experimentally observed *trans* ⟶ *cis* stereopreference.

During recent years organometallic photochemistry has become an area of increasing interest. Owing to the development of sophisticated equipment allowing the detection of intermediates generated by flash photolysis, mechanistic information about photochemical reactions is accumulating increasingly rapidly.[1] Furthermore, an important contribution has also been made by *ab initio* techniques. The calculation of potential-energy surfaces connecting the reactants to the primary products has proven to be a powerful tool in understanding the photochemical processes of a number of simple carbonyl systems,[2–4] such as $[Fe(CO)_5]$, $[CoH(CO)_4]$, $[FeH_2(CO)_4]$ and $[MnH(CO)_4]$.

In this paper we report the results of a self consistent field (SCF) study of the mechanism of the photochemistry of $[Mn(CO)_5Cl]$, a representative of the Group 7A pentacarbonyl halide complexes $[M(CO)_5X]$ (M = Mn or Re; X = Cl, Br or I). The thermal substitution behaviour of this group of complexes has been studied extensively in the past, both experimentally[5,6] and theoretically,[7,8] and the mechanistic details seem well established. However, their photochemical substitution behaviour is more complicated, and, in spite of a great deal of experimental effort,[9–12] a number of questions still remain unanswered.

It has been shown in a number of previous studies that the primary photoprocess for the considered halide complexes is cleavage of an M–CO bond[9–11] [equation (1)]. The subsequent

$$[M(CO)_5X] \xrightarrow{h\nu} [M(CO)_4X] + CO \qquad (1)$$

behaviour of the co-ordinatively unsaturated species formed depends on its surroundings. In the absence of any nucleophilic agent, it will undergo a thermal dimerization reaction (2). The

$$2\,M(CO)_4X \longrightarrow (OC)_4M\begin{matrix}X\\ \diagup\ \diagdown\\ X\end{matrix}M(CO)_4 \qquad (2)$$

dimerization reaction can be prevented if the experiment is performed in the presence of a large amount of CO, or another nucleophilic agent L, which will then co-ordinate to the vacant position of $[Mn(CO)_4X]$, leading to the photosubstitution product $[M(CO)_4X(L)]$ [equation (3)].

$$[M(CO)_4X] + L \longrightarrow [M(CO)_4X(L)] \qquad (3)$$

† *Non-SI units employed:* cal = 4.184 J, au ≈ 5.29 × 10^{-11} m.

In the case of $[Re(CO)_5X]$ (X = Cl, Br or I) in the presence of pyridine (py) or PPh_3 the photosubstitution reaction has been found to be highly stereospecific, yielding only the *cis* isomer[10] [equations (4) and (5)]. The photoproducts are the same as

$$[Re(CO)_5X] + py \xrightarrow{h\nu} cis\text{-}[Re(CO)_4X(py)] + CO \qquad (4)$$

$$[Re(CO)_5X] + PPH_3 \xrightarrow{h\nu} cis\text{-}[Re(CO)_4X(PPh_3)] + CO \qquad (5)$$

those obtained in the thermal substitution reactions of the same compounds. Indeed, it has been shown that the thermal substitution reaction of CO in the $[M(CO)_5X]$ complexes under consideration also leads to a *cis* product.[5,6] There is however a crucial difference between the mechanisms which lead to this product in the thermal and in the photochemical reaction. In the thermal reaction the presence of the halide ligand strongly labilizes the CO group in its *cis* position, and the reaction is 100% stereoretentive in this case. In the photochemical reaction on the other hand, there are strong indications that the leaving CO ligand may be situated *trans* to the halide ligand at least in some cases. Indeed, both in $[Mn(CO)_5X]$ and in $[Re(CO)_5X]$, photodissociation is observed upon irradiation into the first ligand-field band, characterized by population of the $a_1(d_{z^2})$ orbital.[10,11] Furthermore, photochemical *trans*-CO dissociation has been observed[13] during ^{13}CO exchange experiments on $[Mn(CO)_5Br]$. The fact that no *trans* product is observed implies that the axial labilization in these cases is characterized by 100% stereomobility. This has been rationalized[3,10,14] by invoking an excited-state rearrangement of the square pyramid with X in the apical position, along an irreversible Berry pseudorotation path, and resulting in a square pyramid with X in the equatorial position.

In our study the validity of the proposed mechanism will be examined for $[Mn(CO)_5Cl]$. In a previous study[15] we calculated the ligand-field spectrum of the six-co-ordinated parent compound. We have now studied the labilization mode accompanying the lowest ligand-field excitations, using density difference plots and population analysis. Furthermore, we will present a state correlation diagram, connecting the different five-co-ordinated species involved in the primary photoprocess. This diagram will include the square pyramids resulting from either an axial or equatorial CO labilization, and the trigonal bipyramid connecting them. It will also include the optimum ground-state structure, obtained from a bond-angle optimization of the $[Mn(CO)_4Cl]$ species.

Calculations have been performed on the ground states as

Table 1 Comparison of the lowest calculated energy levels of $[Mn(CO)_5Cl]$ and the experimental spectrum of $[Mn(CO)_5X]$ (in MeOH solution)[27] and $[Re(CO)_5X]$ (X = Cl, Br or I) (in EtOH solution).[10] All values are in cm^{-1}

State	SCF energy $[Mn(CO)_5Cl]$	Exptl. $[Mn(CO)_5Cl]$	$[Mn(CO)_5Br]$	$[Mn(CO)_5I]$	$[Re(CO)_5Cl]$	$[Re(CO)_5Br]$	$[Re(CO)_5I]$
$^1A_1$	0						
$^3E_a(xz,yz \longrightarrow z^2)$	18 478				29 240	28 730	26 810
$^3E_b(xz,yz \longrightarrow x^2 - y^2)$	24 811						
$^3B_2(xy \longrightarrow z^2)$	26 208						
$^1E_a(xz,yz \longrightarrow z^2)$	26 230	26 520	26 070	25 000	31 450	30 950	29 760
$^3A_2(xy \longrightarrow x^2 - y^2)$	27 620						
$^1A_2(xy \longrightarrow x^2-y^2)$	32 657			33 600	~33 900	~33 100	~32 100
$^1E_b(xz,yz \longrightarrow x^2 - y^2)$	35 642	37 000	37 000	36 400	~37 000	~37 000	~35 100
$^1B_2(xy \longrightarrow z^2)$	37 782						~36 600

well as on the first excited ligand-field states of both singlet and triplet spin multiplicity. Although there is a general consensus that ligand-field transitions are the precursors of the photochemical reactions of carbonyl complexes,[16] the spin multiplicity of the photoactive state is still under debate. Experimental evidence seems to point in the direction of a triplet state, at least for the analogous $[Cr(CO)_6]$ photochemistry.[17,18] Yet, so far theoretical studies have always been concerned only with singlet excited states.[3,14,19] In this study we will include the lowest triplet states as well. As part of our results we will show that the general patterns of the state correlation diagram for the triplet and the singlet excited states are essentially identical.

Calculational Details

All calculations were performed within the framework of Roothaan's Restricted Open-shell Hartree–Fock (ROHF) formalism,[20] using the SYMOL program.[21] For the first-row atoms C and O we used the (9s5p/5s3p) Huzinaga–Dunning basis sets,[22] and for the Cl atom the (12s,9p/6s5p) non-segmented basis set proposed by Veillard and Dunning.[23] The central Mn atom was described by a (15s11p6d/9s6p4d) non-segmented basis set, introduced in a previous paper.[15]

All calculations were performed using one set of bond distances, namely 2.369 Å for Mn–Cl, 1.841 Å for Mn–C and 1.124 Å for C–O. These are the average bond lengths for $[Mn(CO)_5Cl]$, resulting from different experimental measurements.[24–26] For six-co-ordinated $[Mn(CO)_5Cl]$ all ligand–metal–ligand bond angles were kept at 90°. For the five-co-ordinate $[Mn(CO)_4Cl]$ species the following geometries were calculated: (*i*) a flat square pyramid with Cl in the apical position; (*ii*) a flat square pyramid with Cl in a basal position; (*iii*) a regular trigonal bipyramid with Cl in the equatorial plane. Finally, a bond-angle optimization was performed on the $[Mn(CO)_4Cl]$ $^1A_1$ state, keeping all bond distances fixed, and maintaining C_{2v} symmetry. The bond angles shown were

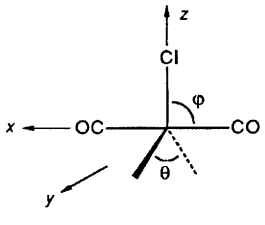

optimized: Cl is situated on the $+z$ axis, φ represents the bond angle between Cl and the CO ligands in the yz plane, while θ is the angle between the two CO ligands in the yz plane. The optimum geometry was reached for θ = 95 and φ = 86°. This structure will be denoted as **I**.

Results and Discussion

Composition and Labilization Mode of the Lowest Triplet and Singlet Excited States.—The calculated transition energies of the lowest ligand-field excited states in $[Mn(CO)_5Cl]$ are shown in Table 1. Also included are the positions of the weak low-energy transitions in the ultraviolet–visible spectra[27] of $[Mn(CO)_5Cl]$, $[Mn(CO)_5Br]$ and $[Mn(CO)_5I]$. These bands were originally assigned as transitions to π*(CO) orbitals;[27] yet in a previous paper[15] we have shown that they should rather be assigned to the symmetry-allowed $^1A_1 \longrightarrow {}^1E$ ligand-field transitions. The lowest transition corresponds to an excitation from the $e(xz,yz)$ shell to the $a_1(z^2)$ orbital, the higher-lying transition to an excitation from $e(xz,yz)$ to the $b_1(x^2 - y^2)$ orbital. The relatively large energy separation of both transitions is connected to the fact that Cl^- is a much weaker σ donor than is CO.[15] As one can see from Table 1, the first band in the spectrum shifts to lower energy in the order $[Mn(CO)_5Cl]$ > $[Mn(CO)_5Br]$ > $[Mn(CO)_5I]$, as can be expected from the position of the halide ligands in the spectrochemical series:[28] Cl > Br > I. The second band is shifted much less between the different spectra. Since this band corresponds to a transition to the $b_1(x^2 - y^2)$ orbital, which is situated in the equatorial plane containing four CO ligands, its position is only dependent on the π-donor properties of the halide ligand. The experimental band positions in Table 1 thus suggest that I is a slightly stronger π donor than are Cl and Br in the complexes considered.

Table 1 also includes the experimental ligand-field bands of the complexes $[Re(CO)_5Cl]$, $[Re(CO)_5Br]$ and $[Re(CO)_5I]$, and their assignment as suggested in ref. 10. Both ^1E bands are also visible here, and their relative position with respect to the heteroligand follows the same trend as for the manganese complexes. The spectrum of the rhenium complexes does however contain a number of additional ligand-field bands: the spin-allowed $^1A_1 \longrightarrow {}^1A_2(xy \longrightarrow x^2 - y^2)$ transition shows up below the ^1E_b band, and, owing to the larger spin–orbit coupling in the rhenium complexes, the spin-forbidden $^1A_1 \longrightarrow {}^3E_a$ transition appears as a shoulder at the low-energy side of the corresponding $^1A_1 \longrightarrow {}^1E_a$ transition.

We now turn to a discussion of the possible photoactive states in the complexes under consideration. As one can see from Table 1, the lowest possible one-electron excitation leads to an occupation of d_{z^2} in all cases. Since most of the chemical reaction is likely to occur from the lowest excited state it is clear that the E_a state, either triplet or singlet, is quite probably the dominant photoactive level. Whether the principal action takes place from a singlet or a triplet state is still a matter of debate. In ref. 29 it was suggested that the central metal ion could play a significant role in this matter. Indeed, as Table 1 shows, the ^3E_a state is populated directly from the ground state in the rhenium complexes, whereas in the manganese complexes it is not. Also, the $[Mn(CO)_5X]$ complexes do not undergo radiative decay, while the rhenium analogues all exhibit $^3E \longrightarrow {}^1A_1$ luminescence.[10]

Table 2 Mulliken orbital populations on the central Mn atom and on the different ligands in the $^1A_1$ ground state and the ^3E_a, ^1E_a, $^3A_2$ and $^1A_2$ excited states of $[Mn(CO)_5Cl]$; Δ is the difference between the excited and the ground state

	$^1A_1$	^3E_a	Δ	^1E_a	Δ	$^3A_2$	Δ	$^1A_2$	Δ
Mn									
s	6.211	6.214	+0.003	6.216	+0.005	6.211	+0.000	6.219	+0.008
p	12.160	12.166	+0.006	12.173	+0.013	12.145	−0.015	12.148	−0.012
d_{z^2}	0.584	1.375	+0.791	1.391	+0.807	0.589	+0.005	0.589	+0.005
$d_{x^2-y^2}$	0.555	0.549	−0.006	0.552	−0.003	1.328	+0.773	1.349	+0.794
$d_{xz,yz}$	3.673	2.754	−0.919	2.721	−0.952	3.598	−0.075	3.646	−0.027
d_{xy}	1.705	1.704	−0.001	1.725	+0.020	0.837	−0.868	0.775	−0.930
CO_{ax}									
ρ	9.749	9.816	+0.067	9.801	+0.052	9.721	−0.028	9.733	−0.016
π	4.238	4.219	−0.019	4.231	−0.007	4.264	+0.026	4.249	+0.011
CO_{eq}									
σ	9.728	9.744	+0.016	9.745	+0.017	9.803	+0.075	9.790	+0.062
π	4.202	4.195	−0.007	4.194	−0.008	4.175	−0.027	4.185	−0.017
Cl									
σ	9.556	9.646	+0.090	9.634	+0.078	9.546	−0.010	9.547	−0.009
π	7.847	7.800	−0.047	7.799	−0.048	7.848	+0.001	7.846	−0.001

However, at least for the rhenium complexes, the $E_a(xz,yz \longrightarrow z^2)$ state is not the only photoactive state involved. From a detailed study[10] on the wavelength dependence of the quantum yield of CO substitution in $[Re(CO)_5X]$ complexes it was concluded that at least two different excited states induce photochemistry. The states involved are the E_a, characterized by a population of d_{z^2} and the A_2 (again either singlet or triplet), corresponding to an $xy \longrightarrow x^2 - y^2$ excitation in the equatorial plane (see Table 1). Both states can be expected to lead to a different photochemical reaction pattern, since they involve the labilization of different CO ligands. Up to now, there seems to be no experimental evidence of any involvement of the other two ligand-field states, $^{1,3}E_b(xz,yz \longrightarrow x^2 - y^2)$ and $^{1,3}B_2(xy \longrightarrow z^2)$ in the photochemistry of the systems under consideration. Therefore, we will not include these states in our discussion.

The labilization of the different ligands can be studied at the *ab initio* level by considering the changes in electron density that are induced by the different excitation processes. These changes are evaluated in Table 2, containing a Mulliken population analysis of the $^1A_1$ ground state and the excited states $^{1,3}E_a$ and $^{1,3}A_2$ in $[Mn(CO)_5Cl]$, and in Figs. 1 and 2, showing the electron-density shifts corresponding to the $^1A_1 \longrightarrow {}^3E_a$ (Fig. 1) and the $^1A_1 \longrightarrow {}^3A_2$ transition (Fig. 2) respectively.

As Fig. 1 shows, the largest density shifts accompanying the $^1A_1 \longrightarrow {}^{1,3}E_a$ transition clearly occur along the axis containing the heteroligand. At the metal the population of d_{z^2} increases at the expense of $d_{xz,yz}$. The population of the $a_1(z^2)$ σ orbital has its repercussions on all σ bonds. As one can see from Table 2, the $^1A_1 \longrightarrow {}^{1,3}E_a$ transition leads to an increasing σ population on all the ligands, implying that all σ bonds are weakened. The largest increase in σ population occurs for the Cl atom. Based on σ arguments alone, one would therefore expect the E_a state to be the precursor of a M–Cl dissociation reaction. The lack of halide substitution in the complexes under consideration can however be rationalized by π arguments. In the e(*xz,yz*) orbital the metal–ligand interaction is bonding for the π-donor Cl, whereas it is antibonding for the π-acceptor CO. Consequently, a depopulation of this orbital will strengthen the Mn–Cl bond but weaken the Mn–CO bond. Furthermore, by the depopulation of the e(*xz,yz*) π level Cl gets the opportunity to exploit its π-donor character more fully. As one can see from Fig. 1 and Table 2, the Cl π orbital is indeed further depopulated in the lowest ligand-field states $^{1,3}E$, as compared to the ground state. The strengthening of the π bond counteracts the σ-bond weakening of the halide ligand, which therefore does not take part in the substitution reaction. For the CO ligands, however, the opposite effect occurs. As CO is a π acceptor, the depopulation of the e(*xz,yz*) level has a negative effect on its π bonding with the metal. This is clear from Fig. 1 and Table 2: the π orbitals of both *cis* and *trans* CO ligands are depopulated in the $^{1,3}E_a$ excited state as compared to the ground state. Both σ and π effects therefore reinforce each other in weakening the M–CO bonds, and their combined effect will lead to CO dissociation in the $^{1,3}E_a$ excited state. It is furthermore clear from Table 2 and from Fig. 1 that the CO ligand *trans* to the halide ligand is labilized much more than the *cis* CO ligands. Based on the present analysis, one must therefore expect a *trans* CO dissociation upon excitation into the lowest ligand-field band.

The σ/π bonding argument used to rationalize axial CO over axial Cl displacement explains why no M–X bond cleavage is observed in the primary photoprocess of the considered halide complexes.[9–11] Moreover, it is further substantiated by the fact that, for the analogous $[W(CO)_5(NH_3)]$ complexes, W–N cleavage is the main result of population of the $a_1(z^2)$ orbital.[30] Indeed, NH_3 is only a σ donor, so that in this case no strengthening of the π bonding on depopulation of the e(*xz,yz*) level is possible.

Based on Table 2 and Fig. 2, an analogous analysis can be made for the $^1A_1 \longrightarrow {}^{1,3}A_2(xy \longrightarrow x^2 - y^2)$ transition. Since this transition involves an excitation in the equatorial plane of the complex, the halide ligand on the axial axis is hardly affected. As one would expect, the largest density shifts now occur at the equatorial CO ligands, *cis* to the halide ligand. The depopulation of the π orbital $b_2(xy)$ in favour of the σ orbital $b_1(x^2 - y^2)$ again results in a weakening of the CO_{cis} ligands through both their σ and π interaction with the metal. As for the CO ligand *trans* to the halide, the figures in Table 2 indicate a smaller effect, which moreover is opposite to the effect on the CO_{cis} ligands. Both the $M–CO_{trans}$ σ and π interactions are slightly strengthened in the $^{1,3}A_2$ excited states. It is therefore clear that the upper excited-state reaction in the $[Re(CO)_5X]$ complexes will involve an $M–CO_{cis}$ bond cleavage.

(*b*) *State Correlation Diagram connecting the Five-co-ordinated Structures.*—The fact that no *trans* product is observed in the photochemical substitution reaction of the complexes under consideration implies that a different stereochemistry is connected with the two possible labilization modes discussed in the previous section: axial labilization is characterized by 100% stereomobility, equatorial labilization by 100% stereoretention. The absence of *trans* products upon irradiation into the first ligand-field band has been rationalized

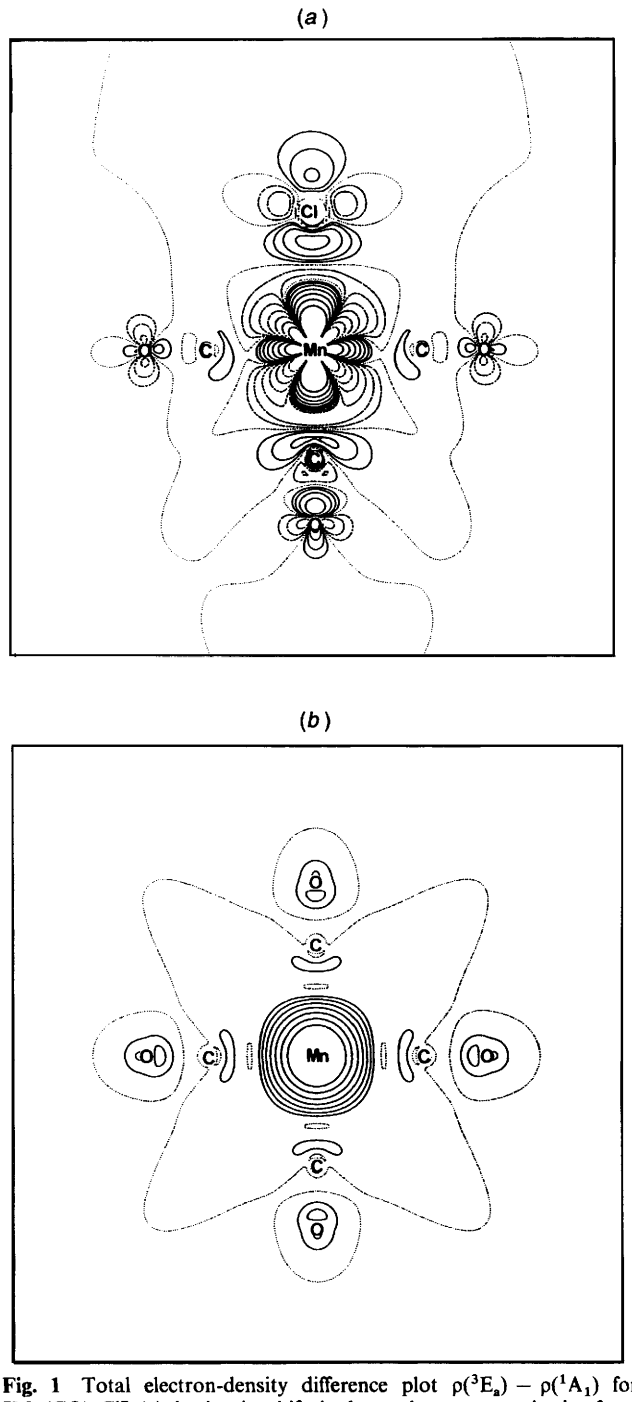

Fig. 1 Total electron-density difference plot $\rho(^3E_a) - \rho(^1A_1)$ for $[Mn(CO)_5Cl]$: (*a*) the density shifts in the *yz* plane upon excitation from the ground state to the photoactive state (the Cl ligand is on the $+z$ axis); (*b*) the corresponding shifts in the *xy* plane. Full contours correspond to an increase in electron density and dashed contours to a decrease. At the dotted lines $\Delta\rho = 0$. The values of the $\Delta\rho$ contours are $\pm 0.001\,25$, ± 0.0025, ± 0.005, ± 0.01, ± 0.02, ± 0.04, ± 0.08 and 0.0 au^{-3}

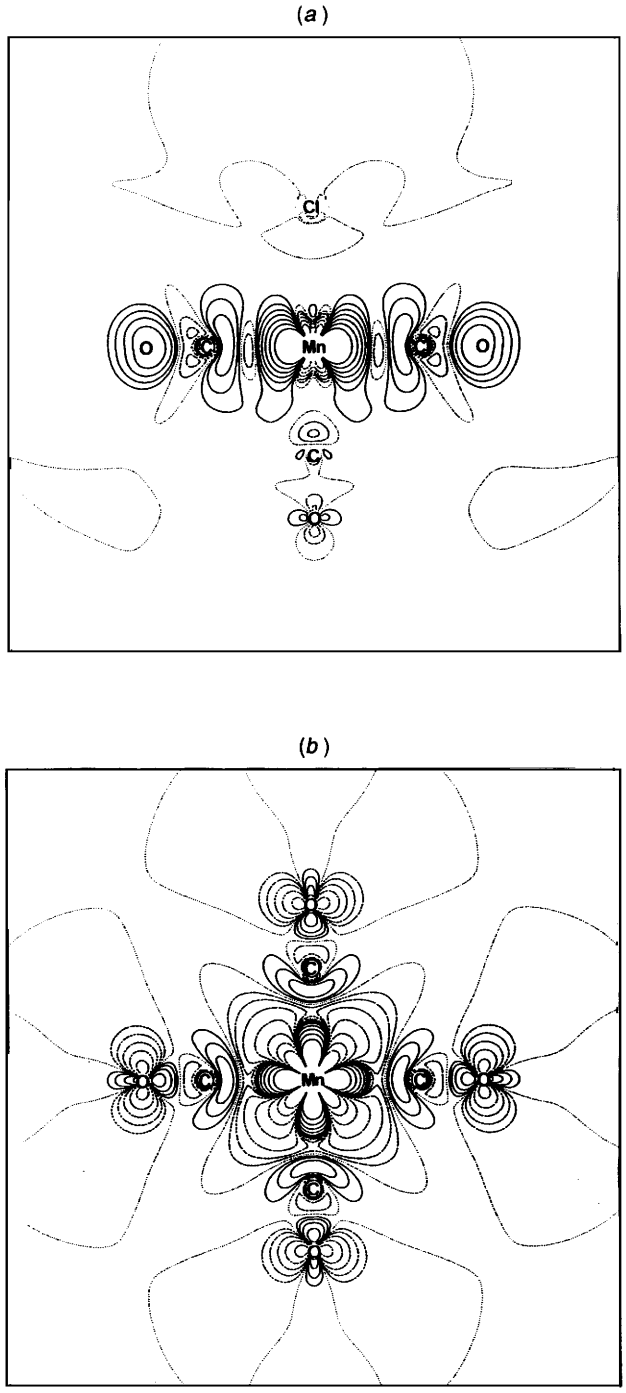

Fig. 2 Total electron-density difference plot $\rho(^3A_2) - \rho(^1A_1)$ for $[Mn(CO)_5Cl]$. Details as in Fig. 1

on several occasions by invoking an excited-state irreversible Berry rearrangement of the square pyramid resulting from *trans*-CO loss (SPY_{ap}), by the mechanism in Scheme 1.

The interconversion proceeds through a trigonal bipyramid

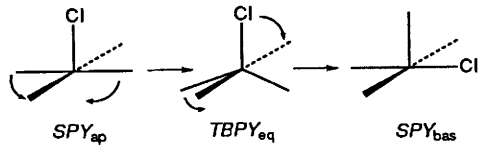

Scheme 1

with the halide ligand in equatorial position ($TBPY_{eq}$), and results in a square pyramid (SPY_{bas}) in which one of the basal CO ligands has exchanged site with the apical halide ligand. Subsequent capture of the nucleophile will now lead to a *cis* product. The SPY_{bas} structure can also be obtained directly from the six-co-ordinated compound by dissociation of a *cis*-CO ligand (although in a different excited state, see below and Fig. 3). Since no stereomobility is observed in this case, the SPY_{bas} must be situated at a minimum on the potential-energy curve connecting the five-co-ordinated species, so that no rearrangement is possible.

In order to investigate the relation between labilization mode and stereochemistry in more detail, Hartree–Fock calculations were performed on the ground state and the lowest excited singlet and triplet states of the relevant $[Mn(CO)_4Cl]$ structures

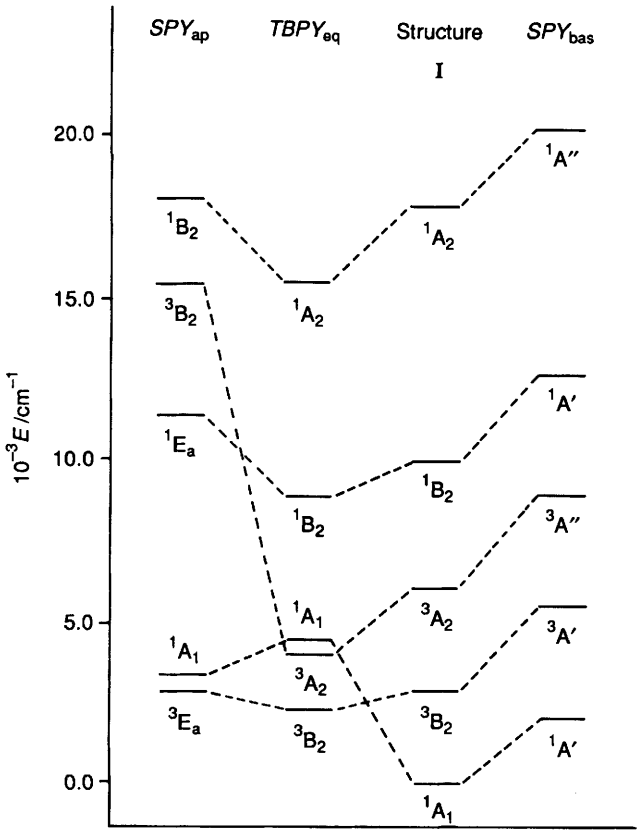

Fig. 3 State correlation diagram, connecting the relevant $[Mn(CO)_4Cl]$ species. The lowest triplet and singlet states are shown corresponding to the states $^1A_1$, $^{3,1}E_a$ and $^{3,1}A_2$ in $[Mn(CO)_5Cl]$. Owing to difficulties with convergence, no SCF energies could be obtained for the highest $^1A'$, and $^1A''$ states of the SPY_{bas} structure. In order to overcome this problem, an additional calculation was performed on the weighted average of all ligand-field states, denoted as $Av(d^6)$. The spectrum of SPY_{bas} structure was then recalculated using the $Av(d^6)$ orbitals. The $Av(d^6)$ energies of the highest $^1A'$, and the $^1A''$ states are shown, relative to the $Av(d^6)$ $^1A'$, ground-state energy. For the latter state, the energy difference between the $Av(d^6)$ energy and the SCF energy amounted to 3750 cm^{-1}

SPY_{ap}, SPY_{bas} and $TBPY_{eq}$. Furthermore, the calculations also included the most stable five-co-ordinated $[Mn(CO)_4Cl]$ species, as specified in the previous section. This structure **I** was shown to be rather close in geometry to $TBPY_{eq}$. In the equatorial plane, the bond angle between the two CO ligands is reduced to 95°, leaving an angle of 142.5° between CO and Cl. The axial axis is also slightly distorted: both axial CO ligands are bent by 4° towards the equatorial Cl ligand.

Fig. 3 shows the energy correlation diagram connecting the four relevant $[Mn(CO)_4Cl]$ species. For convenience, structure **I** is placed in between the $TBPY_{eq}$ and SPY_{bas} structures. In organizing the different species in this way, Fig. 3 becomes a useful tool in elucidating the stereochemistry of both the thermal and stereochemical substitution reactions of the complexes under consideration.

First, consider the correlation surface in Fig. 3, corresponding to the $^1A_1$ ground state of $[Mn(CO)_5Cl]$. This line clearly demonstrates how the thermal release of a CO group *cis* to the Cl ligand is strongly favoured over *trans*-CO loss. The energy difference between the SPY_{ap} and the SPY_{bas} structures amounts to ≈4.0 kcal mol^{-1} (1400 cm^{-1}). Furthermore, equatorial CO loss is strongly assisted by a deformation of the system to generate structure **I**. The same structure cannot be reached during the dissociation of an axial CO group, since the system has to overcome an energy barrier when adopting the $TBPY_{eq}$ structure. The correlation diagram in Fig. 3 thus offers a very simple explanation for the experimentally observed *cis* effect of halide ligands in pentacarbonyl complexes of Mn and Re. It also

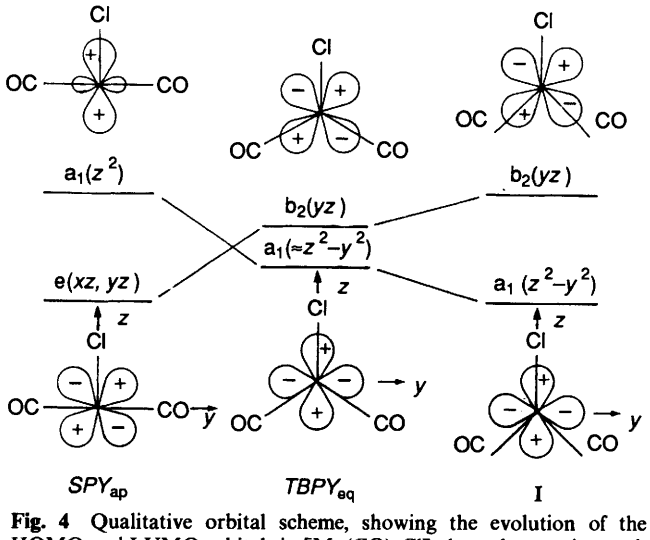

Fig. 4 Qualitative orbital scheme, showing the evolution of the HOMO and LUMO orbitals in $[Mn(CO)_4Cl]$ along the reaction path SPY_{ap} – $TBPY_{eq}$ – structure **I**

demonstrates the highly stereoretentive character of the reaction: after dissociation of a *cis*-CO group, six-co-ordination will necessarily be restored by addition of a nucleophile to structure **I**. The most favourable access path is the equatorial plane, next to the halide ligand.

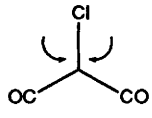

Similar conclusions were also reached in a recent, more detailed, ROHF study of the thermal substitution reaction of $[Mn(CO)_5Cl]$.[8] In this study a complete geometry optimization was performed, both on $[Mn(CO)_5Cl]$ and on the five-co-ordinate $[Mn(CO)_4Cl]$ species that results from either a *trans*- or a *cis*-CO loss. For the fragment that results from a *trans*-CO loss relaxation effects were shown to be unimportant. The optimized structure is very close to a flat square pyramid, with a Cl–M–C angle of 87°. Consequently, relaxation only lowers the activation energy for *trans*-CO loss by 0.9 kcal mol^{-1} (315 cm^{-1}). This will of course hardly affect the qualitative picture offered by Fig. 3. Also, in accord with the present analysis, it was shown that relaxation effects are much more important for the fragment that results from a *cis*-CO dissociation. Due to the fact that no symmetry or bond-length restrictions were imposed during the optimization of the $[Mn(CO)_4Cl]$ fragment, the resulting structure differs slightly from **I**. However, again the qualitative picture offered by Fig. 3 remains valid: in ref. 8 it was found that relaxation lowers the activation energy for *cis*-CO dissociation by 4.1 kcal mol^{-1} (1434 cm^{-1}). This is roughly comparable to the value of 5.7 kcal mol^{-1} (1979 cm^{-1}), obtained in Fig. 3.

The evolution of the $^1A_1$ energy surface between SPY_{ap} and structure **I** can be explained qualitatively by considering the evolution of the highest occupied and lowest unoccupied molecular orbitals (HOMO and LUMO), as illustrated in Fig. 4. Starting from the SPY_{ap} structure, the rearrangement will cause a splitting of the e(*xz*,*yz*) level into $b_1(xz)$ and $b_2(yz)$. Since the deformation essentially takes place in the *yz* plane (see Fig. 4) the $b_1(xz)$ orbital will not be affected very much. The $b_2(yz)$ orbital on the other hand gradually evolves from π bonding to σ antibonding with the equatorial CO ligands, so that its energy will rise drastically. Since this HOMO is doubly occupied in the $^1A_1$ state of the SPY_{ap}, it is responsible for the large initial energy increase of this state. Due to the symmetry lowering from C_{4v} to C_{2v}, the LUMO $a_1(z^2)$ gets a chance to mix with the higher-lying $a_1(x^2 - y^2)$ orbital. Thereby it will

gradually change its character, becoming $(z^2 - y^2)$ like in structure **I**. At the same time it looses its σ-antibonding character with the equatorial CO ligands, and becomes π bonding, thereby steeply decreasing its energy. Consequently, at some point of the rearrangement close to the $TBPY_{eq}$ structure, a crossing must occur between the HOMO and the LUMO. This results in a forbidden crossing between two $^1A_1$ states, so that starting from that point the lowest $^1A_1$ state corresponds to a different configuration, with $a_1(z^2 - y^2)$ doubly occupied. Its energy starts to decrease, and reaches a minimum in Structure **I**, due to the optimal bonding characteristics of the $a_1(z^2 - y^2)$ orbital at this point: π bonding with the CO ligands, σ antibonding with the weak halide ligand.

Since the HOMO–LUMO crossing occurs in the vicinity of the $TBPY_{eq}$ structure, this structure is characterized by a low-lying vacant orbital. As one can see from Fig. 3, this results in a $^3B_2$ ground state, in which both the $b_2(yz)$ and the $a_1(z^2 - y^2)$ orbitals are singly occupied. The $^3B_2$ ground state of $TBPY_{eq}$ correlates with the ^3E_a ground state of the SPY_{ap} structure, which is in turn directly correlated to the ^3E_a excited state of $[Mn(CO)_5Cl]$. The corresponding correlations can of course also be derived for $^1B_2$ and ^1E_a states. The corresponding correlation lines in Fig. 3 must therefore be used to rationalize the stereochemistry of CO photodissociation upon excitation into the $^{3,1}E_a$ ligand-field state. An inspection of these surfaces leads to a very simple analysis.

(*i*) As discussed in the previous section, excitation of $[Mn(CO)_5Cl]$ into the $^{1,3}E_a$ state is followed by the elimination of an axial CO ligand.

(*ii*) As opposed to the ground-state situation, photolytic splitting of CO_{ax} is assisted by a deformation of the SPY_{ap} structure to generate the $TBPY_{eq}$ structure. The latter structure is now situated at a minimum of the potential-energy curve.

(*iii*) An increasing potential-energy curve prevents the system from continuing on the same energy surface, towards structure **I** or possibly towards SPY_{bas}. The $[Mn(CO)_4Cl]$ species therefore gets trapped in the potential well, corresponding to the $^{1,3}B_2$ state. Intersystem crossing will eventually bring it from $^1B_2$ to $^3B_2$. From there it can, however, with only a slight rearrangement, make the transition to the $^1A_1$ potential energy surface. Further rearrangement will then transform it into structure **I**.

(*iv*) Exactly as for the thermal substitution reaction discussed above, six-co-ordination will be restored from structure **I**, with the incoming nucleophile in *cis* position to the halide.

The analysis of the CO substitution following the higher-energy $^1A_1 \longrightarrow {}^{3,1}A_2$ excitation can be carried out in a similar way.

(*i*) We now have to consider the elimination of an equatorial CO ligand. Thereby, the symmetry of the system is reduced from C_{4v} to C_s.

(*ii*) If the geometry of the $[Mn(CO)_4Cl]$ moiety were kept frozen during equatorial CO loss from the six-co-ordinated species, the system would end up at the right-hand side of Fig. 3, in the lowest $^{1,3}A''$ state of the SPY_{bas}. It is however obvious from the figure that a concerted dissociation–rearrangement path will be preferred, leading to the $TBPY_{eq}$ $^{3,1}A_2$ state.

(*iii*) The system is now trapped in a very deep potential well. Intersystem crossing can however again transfer it to the $^1A_1$ surface, possibly passing through the $^3B_2$ ground state of the $TBPY_{eq}$.

(*iv*) The association of structure **I** with an incident nucleophile will again lead to a *cis* product.

Finally, it is worthwhile to situate the photochemical reaction mechanism illustrated in Fig. 3 in a more global picture of strong-field d^6 photostereochemistry. A Berry pseudorotation mechanism has also been proposed to explain the photostereochemistry of other, Werner-type, strong field d^6 complexes (disubstituted amine and cyanide complexes of Co^{III}, Rh^{III} and Ir^{III}).[31,32] However, the photochemical substitution and isomerization reactions of these complexes shows the opposite

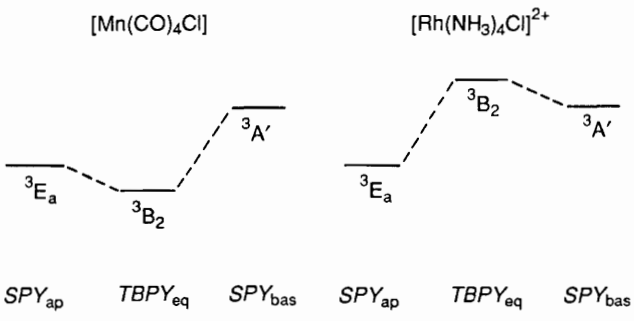

Scheme 2

stereochemical behaviour: *trans* complexes tend to react in a stereoretentive way, while the substitution of *cis* complexes is characterized by *cis* ⟶ *trans* stereomobility. Based on ligand-field arguments it was shown[31] that Berry rotation essentially takes place at the lowest triplet state of the five-co-ordinate species (the lowest triplet potential-energy surface in Fig. 3).

The difference between the stereochemical behaviour of Werner-type strong-field d^6 complexes and the carbonyl complexes considered in this paper can be illustrated by Scheme 2, comparing the energy evolution of the lowest triplet level between the relevant five-co-ordinated structures $[Mn(CO)_4Cl]$ and $[Rh(NH_3)_4Cl]^{2+}$.[31] In both cases, the $^3A'$ state of the SPY_{bas} structure is situated at a significantly higher energy than is the ^3E_a state of SPY_{ap}. However, the $TBPY_{eq}$ ground state is situated at a minimum of the energy surface in the carbonyl complexes (see also Fig. 3), whereas in the Werner-type complexes it is a transition state, with the two square pyramids as local minima on both sides. Both square pyramids can then in principle act as deactivation funnels. However, since the energy well is definitely deeper on the side of the SPY_{ap} structure, the latter will determine the dominant product geometry. Six-co-ordination will now mainly be restored by association of a solvent molecule with the SPY_{ap} ground state, leading to a *trans* product.

Our calculations are in accord with the result of an extended-Hückel analysis of the photolysis of $[Cr(CO)_6]$,[19] in that the $[Cr(CO)_5]$ excited energy surface also reaches a minimum at *TPBY* structure. However, a previous *ab initio* analysis of the photolysis of the very analogous complexes $[Tc(CO)_5Cl]$, $[Mo(CO)_5Me]$ and $[Mo(CO)_5(PMe_3)]$[14] led to a strikingly different result. This analysis was performed on the lowest excited singlet level [the $^1E_a(SPY_{ap})$–$^1B_2(TBPY_{eq})$–$^1A'(SPY_{bas})$ surface in Fig. 3]. Yet, the calculations led to a completely differently shaped energy surface, with the SPY_{bas} structure situated at a minimum, the SPY_{ap} at a maximum, and the $TBPY_{eq}$ structure in between them. The reason for this discrepancy is not clear to us. It might partially be caused by the fact that the calculations on the complexes of Tc and Mo were performed with a relatively small basis set. Yet this discrepancy raises some doubt as to how far the present analysis remains valid for photolysis of the second- and third-row monosubstituted carbonyl complexes $[Tc(CO)_5X]$ and $[Re(CO)_5X]$. In order to get a final answer additional calculations on these systems will be necessary.

Conclusion

The observed photochemical behaviour of $[Mn(CO)_5Cl]$ and other Group 7A pentacarbonyl halide complexes can be rationalized satisfactorily at the Hartree–Fock level.

From an analysis of the electron-density shifts that occur upon excitation to the two photoactive states ($^{1,3}E_a$ and $^{1,3}A_2$) it was shown that the dominant reaction modes are axial CO loss in the $^{1,3}E_a$ state and equatorial CO loss in the $^{1,3}A_2$ state.

The observed stereochemical *trans* ⟶ *cis* preference can be rationalized by a Woodward–Hoffmann correlation diagram, connecting the relevant five-co-ordinate $[Mn(CO)_4Cl]$ struc-

tures. It was shown that the $TBPY_{eq}$ structure is situated at a minimum of the excited-state surface, both in the case of axial and equatorial CO labilization. It will therefore act as a trap, bringing the system back to the $^1A_1$ energy surface by intersystem crossing. Six-co-ordination will then be restored by the attack of the incoming nucleophile on a distorted *TBPY* structure I, leading to a *cis* product.

Acknowledgements

The authors are indebted to the Belgian National Fund for Scientific Research and to the Belgian Government (Programmatie van het Wetenschapsbeleid) for financial support.

References

1 M. Poliakoff and E. Weitz, *Adv. Organomet. Chem.*, 1986, **25**, 277.
2 C. Daniel, M. Bénard, A. Dedieu, R. Wiest and A. Veillard, *J. Phys. Chem.*, 1984, **88**, 4805.
3 A. Veillard, C. Daniel and A. Strich, *Pure Appl. Chem.*, 1988, **60**, 215.
4 C. Daniel, *Coord. Chem. Rev.*, 1990, **97**, 141.
5 J. D. Attwood and T. L. Brown, *J. Am. Chem. Soc.*, 1975, **97**, 3380.
6 J. D. Attwood and T. L. Brown, *J. Am. Chem. Soc.*, 1976, **98**, 3160.
7 D. L. Lichtenberger and T. L. Brown, *J. Am. Chem. Soc.*, 1978, **100**, 366.
8 R. D. Davy and M. B. Hall, *Inorg. Chem.*, 1989, **28**, 3524.
9 C. H. Bamford, J. W. Burley and M. Coldbeck, *J. Chem. Soc., Dalton Trans.*, 1972, 1846.
10 M. S. Wrighton, D. L. Morse, H. B. Gray and D. K. Ottesen, *J. Am. Chem. Soc.*, 1976, **98**, 1111.
11 X. Pan, C. E. Philbin, M. P. Castellani and D. R. Tyler, *Inorg. Chem.*, 1988, **27**, 671.
12 T. M. McHugh, A. J. Rest and D. J. Taylor, *J. Chem. Soc., Dalton Trans.*, 1980, 1803.
13 A. Berry and T. Brown, *Inorg. Chem.*, 1972, **11**, 1165.
14 C. Daniel and A. Veillard, *Nouv. J. Chim.*, 1986, **10**, 83.
15 K. Pierloot, P. Hoet and L. G. Vanquickenborne, *Inorg. Chim. Acta*, in the press.
16 G. L. Geoffroy and M. S. Wrighton, *Organometallic Photochemistry*, Academic Press, New York, 1979.
17 A. Vogler, *Z. Naturforsch, Teil B*, 1970, **25**, 1069.
18 J. Nasielski and A. Colas, *Inorg. Chem.*, 1978, **17**, 237.
19 J. K. Burdett, J. M. Grzybowski, R. N. Perutz, M. Poliakoff, J. J. Turner and R. F. Turner, *Inorg. Chem.*, 1978, **17**, 147.
20 C. C. J. Roothaan, *Rev. Mod. Phys.*, 1960, **32**, 179.
21 G. A. Van der Velde, Ph.D. Thesis, Rijksuniversiteit Groningen, 1974.
22 T. H. Dunning, *J. Chem. Phys.*, 1970, **53**, 2823; S. Huzinaga, *J. Chem. Phys.*, 1965, **42**, 1293.
23 A. Veillard, *Theor. Chim. Acta*, 1968, **12**, 405; T. H. Dunning, *Chem. Phys. Lett.*, 1970, **7**, 423.
24 S. J. La Placa, W. C. Hamilton, J. A. Ibers and A. Davidson, *Inorg. Chem.*, 1969, **8**, 1928.
25 R. F. Bryan, P. T. Green and A. R. Manning, *Abstracts of the American Crystallographic Association*, Seattle, WA, March 1969, M6.
26 P. T. Greene and R. F. Bryan, *J. Chem. Soc. A*, 1971, 1559.
27 G. B. Blakney and W. F. Allen, *Inorg. Chem.*, 1971, **10**, 2763.
28 M. Gerloch and R. C. Slade, *Ligand-field parameters*, Cambridge University Press, 1973.
29 W. F. Allen, *Inorg. Chem.*, 1974, **13**, 905.
30 M. Wrighton, *Chem. Rev.*, 1974, **74**, 401.
31 L. G. Vanquickenborne and A. Ceulemans, *Inorg. Chem.*, 1978, **17**, 2730.
32 L. G. Vanquickenborne and A. Ceulemans, *Coord. Chem. Rev.*, 1983, **48**, 157.

Received 14*th February* 1991; *Paper* 1/00701G